Published in final edited form as:
J Acoust Soc Am. 2003 September ; 114(3): 1462–1466.

Outer hair cell piezoelectricity: Frequency response enhancement and resonance behavior

Erik K. Weitzel,
Bobby R. Alford Department of Otorhinolaryngology and Communicative Sciences, Baylor College of Medicine, Houston, Texas 77030

Ron Tasker, and
TASI Technical Software, Inc., 444 Frontenac Street, Kingston, Ontario K7L 3T4, Canada

William E. Brownell[a)]
Bobby R. Alford Department of Otorhinolaryngology and Communicative Sciences, Baylor College of Medicine, Houston, Texas 77030

Abstract

Stretching or compressing an outer hair cell alters its membrane potential and, conversely, changing the electrical potential alters its length. This bi-directional energy conversion takes place in the cell's lateral wall and resembles the direct and converse piezoelectric effects both qualitatively and quantitatively. A piezoelectric model of the lateral wall has been developed that is based on the electrical and material parameters of the lateral wall. An equivalent circuit for the outer hair cell that includes piezoelectricity shows a greater admittance at high frequencies than one containing only membrane resistance and capacitance. The model also predicts resonance at ultrasonic frequencies that is inversely proportional to cell length. These features suggest all mammals use outer hair cell piezoelectricity to support the high-frequency receptor potentials that drive electromotility. It is also possible that members of some mammalian orders use outer hair cell piezoelectric resonance in detecting species-specific vocalizations.

I. INTRODUCTION

Early in the 1880s, Jacques and Pierre Curie reported that the application of mechanical stress to one of a variety of crystalline materials produced electricity and coined the term piezoelectricity (from the Greek, *piezein*—to press). After considering the thermodynamics of the process, Gabriel Lippmann concluded that applying an electric field across the crystals should produce mechanical stress. The Curie brothers quickly confirmed the converse piezoelectric effect predicted by Lippmann (Cady, 1946). Crystalline piezoelectric materials have been used in applications that range from marine sonar to mechanical actuators to electronic delay lines. Noncrystalline, biological piezoelectricity has been observed in bone (Fukada and Yasuda, 1957) and ligament (Korostoff, 1977; Fukada, 1982).

Outer hair cell (OHC) electromotility (Brownell *et al.*, 1985) is a direct conversion of membrane potential to cell length change and is functionally equivalent to the converse piezoelectric effect. The mechanism responsible for electromotility resides in the OHC lateral wall, a nanoscale composite of membranes and cytoskeletal proteins (Brownell *et al.*, 2001).

[a)]Author to whom correspondence should be addressed at One Baylor Plaza NA 505, Houston, TX 77030. brownell@bcm.tmc.edu

PACS numbers: 43.38.Fx, 43.64.Bt, 43.64.Ld [WPS]

The OHC lateral wall also supports a mechanoelectrical conversion (the direct piezoelectric effect) (Gale and Ashmore, 1994; Zhao and Santos-Sacchi, 1999), which further strengthens the view that the lateral wall is piezoelectric. Several theoretical treatments of the OHC and its role in hearing have assumed the OHC to be piezoelectric (Mountain and Hubbard, 1994; Tolomeo and Steele, 1995; Spector *et al.*, 1998, 1999; Raphael *et al.*, 2000; Iwasa, 2001; Spector *et al.*, 2002). The models all infer or assume Maxwell reciprocity (Cady, 1946) in which the coefficients for the direct and converse effects are equal. Recent experimental evidence provides quantitative support for this thermodynamic requirement for piezoelectricity (Dong *et al.*, 2002).

Electomotility makes a major contribution to the sensitivity and frequency selectivity of mammalian hearing (Brownell *et al.*, 2001; Liberman *et al.*, 2002). The motor mechanism responsible is membrane based, does not depend on calcium or cellular stores of ATP, and is capable of generating mechanical force at frequencies >50 kHz (Brownell and Kachar, 1986; Kachar *et al.*, 1986; Frank *et al.*, 1999; Brownell *et al.*, 2001). The functional significance of electromotility has been questioned because an equivalent circuit analysis based on conventional membrane resistance and capacitance predicts a low-pass frequency response that would limit the membrane voltage and therefore force production only to low frequencies (Hudspeth and Logothetis, 2000). We show that the inclusion of piezoelectricity into the equivalent circuit of the outer hair cell pushes the corner frequency to higher values. In addition, piezoelectric materials can be driven into resonance and we present an analysis predicting resonance in OHCs in the ultrasonic range. The predicted values are, however, compatible with those used for echolocation in chiroptera (bats) and cetaceans (whales and dolphins).

II. METHODS

Lateral wall piezoelectricity is modeled for two different representations of the outer hair cell lateral wall, a rectangular slab and a cylindrical shell. The piezoelectric and material properties are assumed to be homogenous for both geometries. The rectangular slab is known as a length-thickness extension (LTE) resonator in the piezoelectric literature. Most of our analysis is developed for the LTE model because its properties are the most thoroughly studied. The cylindrical shell more closely matches the geometry of the OHC lateral wall and it is called a radial-poled cylinder (RPC) resonator.

III. RESULTS

For the purpose of analysis, the OHC lateral wall is split along its length and rolled out to form a rectangular slab detached from other cellular elements (Fig. 1). The slab is laid out along three Cartesian axes. The circumference of the cylinder is represented by the width (w) of the slab, parallel to x_2; the cell length (l) and wall thickness (t) are parallel to x_1 and x_3, respectively. The lateral wall is a composite structure composed of the plasma membrane, cortical lattice, and subsurface cisterna. OHC electromotility involves electromechanical coupling between all three layers (Brownell *et al.*, 2001) and we assume a thickness of 100 nm (seen in electron micrographs). An electric field across the lateral wall defines the direction of poling or net polarization across the thickness (t) of the slab (x_3 direction) and the resonance mode of interest induced by this field is along the length of the cell (x_1 direction). This is a LTE resonator the properties of which are fully described in the IEEE standard (Rosen *et al.*, 1992). The pertinent constitutive piezoelectric equations are

$$S = s^E T - dE, \qquad D = dT + \varepsilon_0 \varepsilon^T E, \tag{1}$$

where S is the strain, D is the electric polarization (or displacement), s^E is the elastic compliance at constant electric field, ε_0 is the permittivity of free space, ε^T is the permittivity coefficient of the slab at constant stress, T is the stress, E is the electric field, and d is the piezoelectric constant of the slab. Equation (1) is a set of tensor equations, having electrical and mechanical properties in three dimensions where the mechanical properties include shear. The off-diagonal coefficients (d) are the same, as required by Maxwell reciprocity, and, specifically, $d_{31}=d_{13}$ in the complete LTE tensor representation (Rosen *et al.*, 1992). For a thin plate, $t \ll l$, the LTE resonator can be represented by a plane electrical wave propagating in the thickness direction coupled to a plane mechanical wave propagating in the length direction and Eq. (1) becomes

$$S_1=s_{11}^E T_1 - d_{31}E_3, \qquad D_3=d_{31}T_1+\varepsilon_0\varepsilon_{33}^T E_3. \tag{2}$$

For unclamped standing waves in the length-direction, stress is zero at the ends of the specimen and S_1 becomes a function only E_3. The two parts of Eq. (2) are used to solve for D_3. Current as a function of frequency (f) is determined by integrating D_3 with respect to time. Dividing by voltage, we obtain the admittance of the specimen:

$$\begin{aligned} Y(f) = \; & i\frac{2\pi f l w}{t}\left(\varepsilon_0\varepsilon_{33}^T - \frac{d_{31}^2}{s_{11}^E}\right) \\ + \; & i\frac{2wd_{31}^2}{ts_{11}^E\sqrt{\rho s_{11}^E}}\tan\left(\pi f l\sqrt{\rho s_{11}^E}\right). \end{aligned} \tag{3}$$

See Table I for definitions of the symbols. The first term in $Y(f)$ after expanding the right side, reveals a conventional dependence on the E field while the 2nd and 3rd terms result from the dependence of S on E. Note that the quantity $\sqrt{\rho s_{11}^E}$ is the inverse of the speed of sound in the lateral wall.

Experimental values for the coefficients (Table I) are obtained from the literature (Halter *et al.*, 1997;Spector *et al.*, 1998,1999). There have been no direct measures of the elastic compliance (s_{11}^E) and the piezoelectric coefficient (d_{31}^2) for the lateral wall. The first may be calculated from a one-dimensional determination of the axial Young's modulus (Y_{11}) for the OHC modeled as a spring with spring constant (k_1). A range of values for the axial Young's modulus has been reported and we choose one that is near the mean. It was obtained by compressing the OHC with a calibrated cantilever without controlling the membrane potential (Holley and Ashmore, 1988). The elastic compliance of a hollow cylinder of length (l), width w), radius (r), and thickness (t) is

$$s_{11}^E=Y_{11}^{-1}=\frac{\text{strain}}{\text{stress}}=\frac{\Delta L_1/L_1}{F_1/A}=\frac{\Delta L_1/L_1}{k_1\Delta L_1/A}=\frac{A}{k_1L_1}, \tag{4}$$

where $A=\pi(r)^2-\pi(r-t)^2\approx 2\pi\, rt=wt$ and $L_1=l$. The piezoelectric coefficient d_{31}^2 is calculated from

$$d_{31}=\frac{\text{strain}_1}{\text{ElectricField}_3}=\frac{\Delta L_1/L_1}{V_3/t}=\frac{S_1}{V_3}t. \tag{5}$$

The values for S_1/V_3 (Where V_3 is the potential difference across the wall thickness) are available from the literature (Tolomeo and Steele, 1995).

An equivalent circuit of the OHC that included piezoelectricity was developed to evaluate its influence on the membrane potential. A model of current flow across OHC membranes for a cell held in a microchamber (Dallos and Evans, 1995) was adapted. The model retained the two-dimensional radially symmetric RC circuit of the original, with a piezoelectric element (Sherrit *et al.*, 1997) added in parallel to the lateral wall membrane resistance (Fig. 2). The admittance of the element is that defined for the LTE model in Eq. (3). The element is added in parallel because the piezoelectric element is assumed to be an ideal material with no losses so that there would be no current at DC. Two simulations were performed (1) with piezoelectricity and (2) with a capacitor (the membrane capacitance alone).

The results of these simulations are seen in Fig. 3 in which the voltage-divider equivalent impedance is plotted against frequency. Piezoelectricity pushes the corner frequency to a higher value and diminishes the magnitude of dampening. Figure 3 also provides a comparison between cells of different length (20 vs 80 μm). Resonance and corner frequencies are increased in the shorter cell while the overall electrical behavior is similar.

Based on the IEEE-defined formula for the series resonance frequency $f_s = (1/2l)\sqrt{1/\rho s_{11}^E}$, the first resonance frequency for the piezoelectric slab (80 μm) is predicted at 37 kHz. An iterative solution of

$$\frac{\left(k_{31}^l\right)^2}{1-\left(k_{31}^l\right)^2} = \frac{\pi}{2}\frac{f_p}{f_s}\tan\left(\frac{\pi}{2}\frac{\Delta f}{f_s}\right)$$

predicts the anti-resonance frequency (f_p) at 46 kHz, where $\left(k_{31}^l\right)^2 = d_{31}^2/\varepsilon_{33}^T s_{11}^E$ is the electromechanical coupling constant. Additional confirmation of OHC piezoelectricity would come from comparing impedance and admittance in isolated cells to confirm a shift between resonance (f_s) and antiresonance (f_p). Resonance frequencies increase with decreasing cell length (Fig. 4). This is intuitive as resonance frequency is inversely proportional to length for most materials. An inverse relationship was also found between resonance frequency and slab thickness (Fig. 5).

A radial-poled cylinder (RPC) resonator (Ebenezer and Sujatha, 1997) was also examined. It allowed an assessment of not considering the contribution of S_2 resonance mode in the development of the LTE model. The RPC model consists of a cylindrical shell where the diameter of the cylinder is much greater than the thickness of the shell and the electric field acts across the shell thickness. The d_{31} coefficient defined in the LTE mode) couples to the circumferential direction causing a displacement (described by s_{11}^E) manifesting itself as a hoop or breathing mode. This then couples to the length of the cylinder through s_{12}^E to result in the radialpoled cylinder resonator. The resonance spectra of different length radial-poled cylinders were nearly identical to those of the rectangular slab model when l (Cell length)>60 μm. The resonance of shorter cylinders was less than that of the same length LTE model (Fig. 6), showing that inclusion of an S_2 resonance mode becomes more important in the LTE model as l becomes shorter.

IV. DISCUSSION

An unresolved challenge to the OHC's role as the cochlear amplifier has been the fact that a conventional circuit analysis based on passive resistive and capacitive elements predicts a low-pass behavior as with the dashed curves in Fig. 3 (Hudspeth and Logothetis, 2000). This should

restrict OHC electromotility to low frequencies below a corner frequency determined by the length of the cell. A thermodynamic approach suggests a piezoelectric augmentation of the OHC receptor potential that results from the OHC deformation that occurs during normal cochlear vibrations (Spector *et al.*, 2002,2003). The present results, based on an engineering analysis of the lateral wall, reveal that OHC piezoelectricity would also extend the frequency range of stereocilia mediated sensory receptor currents. Electromotility is mediated by the transmembrane receptor potential. Future cochlear modeling should consider the contributions to the OHC receptor potential from both ionic currents and piezoelectric modulation of the membrane potential by acoustically driven cell deformation.

The extended frequency range predicted from our model is consistent with the corner frequencies measured for mechanically unloaded OHCs when stimulated in the microchamber configuration (Dallos and Evans, 1995; Frank *et al.*, 1999). Even though a mechanical resonant peak has not been observed in isolated OHCs, Frank *et al.* (1999) attributed the electrically induced displacement response, with its elevated cutoff frequency, to the presence of a second-order resonance. This conclusion was based on fitting the displacement response, in both amplitude and phase, with that of an over-damped second-order resonant system, in which the resonant frequency was found to depend on cell length. Their data required the presence of a length-dependent resonance similar to that shown in Fig. 4.

The OHC is mechanically loaded in the fluid filled organ of Corti. It is firmly anchored to supporting cells by tight junctions in the reticular lamina. The tectorial and basilar membranes introduce additional mechanical loads. The *in vivo* OHC is therefore a viscous-damped mechanically loaded resonator in contrast to the unloaded or free resonator in our analysis. Radiation damping of the resonance would be expected to result in a broadening and weakening of the impedance peak as a function of frequency. The observation of a broad, ultrasonic mechanical resonance in electrically evoked basilar membrane vibrations near the round window of the guinea pig inner ear (Grosh *et al.*, 2003) is consistent with this expectation. The OHCs near the round window are all short and close to the same length. By inference they should have similar resonance behavior. Electrical stimulation around this frequency would result in a summed response that would be broader than that expected in an unloaded OHC. Many rodents display ultrasonic vocalizations during mating (White *et al.*, 1998). The broad electrically evoked ultrasonic vibrations observed in the guinea pig ear (Grosh *et al.*, 2003) contain these mating frequencies.

Outer hair cells appeared with mammals over 200 million years ago. The OHCs of the small rodentlike early mammals enabled them to hear frequencies above 50 kHz. They were the basis of a cochlear amplifier that counteracted viscous damping and refined the passive mechanical filtering of the organ of Corti (Brownell *et al.*, 2001). Hair cell resonance would not benefit hearing in most mammals and it is of interest that the predicted resonance frequencies are generally beyond the frequency range that OHCs at a specific location on the basilar membrane would operate. In addition, the impedance mismatch between the OHCs and the organ of Corti is so severe that any resonance would be expected to remain confined within the cell and have little impact on the vibrations of the organ of Corti. The importance of OHC biological piezoelectricity for all mammals appears to be its ability to improve the high-frequency electrical response and allow the cochlear amplifier to work throughout the mammalian frequency range.

The first bats appeared over 60 million years ago with an elegant echolocation mechanism that allowed them to navigate in a nocturnal environment. An additional resonance has been invoked to explain their enhanced hearing sensitivity at the echolocation frequencies (Kossl and Russell, 1995; Russell and Kossl, 1999). Bats may have co-opted OHC piezoelectric resonance to achieve this. Some 10 million years later cetaceans adopted a remarkably similar

specialization (Ketten, 1997). The organ of Corti in echolocating members of the orders *chiroptera* and *cetacea* is greatly expanded at the region devoted to the echolocation frequencies. The OHCs in the region are short and of uniform length so that the reticular lamina is parallel to the basilar membrane. This organization would allow OHC resonance to be summed, overcoming the impedance mismatch that normally obscures the resonance. While echolocating mammals may be the only ones to utilize the cellular resonance, the piezoelectric mechanism that underlies it helps to support high-frequency receptor potentials throughout the entire class *mammalia*.

Acknowledgments

Research supported by National Science Foundation Nanotechnology Initiative Research Grant No. BES-9871994 and Public Health Service Research Grant No. DC 00354 from NIDCD. The authors would like to thank Dr. Grosh, Dr. Gummer, Dr. Oghalai, Dr. Rabbitt, Dr. Raphael, and Dr. Spector for helpful comments and Nainesh Gandhi for his assistance with data entry in the cylindrical model.

References

Brownell, WE.; Kachar, B. Outer hair cell motility: A possible electro-kinetic mechanism. In: Allen, JB.; Hall, JL.; Hubbard, AE.; Neely, ST.; Tubis, A., editors. Peripheral Auditory Mechanisms. Springer-Verlag; Berlin: 1986. p. 369-376.

Brownell WE, Bader CR, Bertrand D, de Ribaupierre Y. Evoked mechanical responses of isolated cochlear outer hair cells. Science 1985;227:194–196. [PubMed: 3966153]

Brownell WE, Spector AA, Raphael RM, Popel AS. Micro- and Nanomechanics of the Cochlear Outer Hair Cell. Annu. Rev. Biomed. Eng 2001;3:169–194. [PubMed: 11447061]

Cady, WG. Piezoelectricity. McGraw-Hill; New York: 1946.

Dallos P, Evans BN. High-frequency motility of outer hair cells and the cochlear amplifier. Science 1995;267:2006–2009. [PubMed: 7701325]

Dong XX, Ospeck M, Iwasa KH. Piezoelectric reciprocal relationship of the membrane motor in the cochlear outer hair cell. Biophys. J 2002;82:1254–1259. [PubMed: 11867442]

Ebenezer DD, Sujatha AJ. New methods to characterize radially polarized piezoelectric ceramic cylindrical shells of finite length. J. Acoust. Soc. Am 1997;102:1540–1548.

Frank G, Hemmert W, Gummer AW. Limiting dynamics of high-frequency electromechanical transduction of outer hair cells. Proc. Natl. Acad. Sci. U.S.A 1999;96:4420–4425. [PubMed: 10200277]

Fukada E. Electrical phenomena in biorheology. Biorheology 1982;19:15–27. [PubMed: 7093449]

Fukada E, Yasuda I. On the piezoelectric effect of bone. J. Phys. Soc. Jpn 1957;12:1158–1162.

Gale JE, Ashmore JF. Charge displacement induced by rapid stretch in the basolateral membrane of the guinea-pig outer hair cell. Proc. R. Soc. London, Ser. B 1994;255:243–249.

Grosh, K.; Zheng, J.; deBoer, E.; Nuttall, AL. personal communication. 2003. High frequency electromotile responses in the cochlea.

Halter JA, Kruger RP, Yium MJ, Brownell WE. The influence of the subsurface cisterna on the electrical properties of the outer hair cell. NeuroReport 1997;8:2517–2521. [PubMed: 9261819]

Holley MC, Ashmore JF. A cytoskeletal spring in cochlear outer hair cells. Nature (London) 1988;335:635–637. [PubMed: 3173482]

Hudspeth AJ, Logothetis NK. Sensory systems. Curr. Opin. Neurobiol 2000;10:631–641. [PubMed: 11084326]

Iwasa KH. A two-state piezoelectric model for outer hair cell motility. Biophys. J 2001;81:2495–2506. [PubMed: 11606265]

Kachar B, Brownell WE, Altschuler RA, Fex J. Electrokinetic shape changes of cochlear outer hair cells. Nature (London) 1986;322:365–368. [PubMed: 3736662]

Ketten DR. Structure and function in whale ears. Bioacoustics 1997;8:103–135.

Korostoff E. Stress generated potentials in bone: relationship to piezoelectricity of collagen. J. Biomech 1977;10:41–44. [PubMed: 845176]

Kossl M, Russell IJ. Basilar membrane resonance in the cochlea of the mustached bat. Proc. Natl. Acad. Sci. U.S.A 1995;92:276–279. [PubMed: 7816832]

Liberman MC, Gao J, He DZ, Wu X, Jia S, Zuo J. Prestin is required for electromotility of the outer hair cell and for the cochlear amplifier. Nature (London) 2002;419:300–304. [PubMed: 12239568]

Mountain DC, Hubbard AE. A piezoelectric model of outer hair cell function. J. Acoust. Soc. Am 1994;95:350–354. [PubMed: 8120246]

Raphael RM, Popel AS, Brownell WE. A membrane bending model of outer hair cell electromotility. Biophys. J 2000;78:2844–2862. [PubMed: 10827967]

Rosen, CZ.; Hiremath, BV.; Newnham, R. Piezoelectricity. American Institute of Physics; New York: 1992. IEEE standard on piezoelectricity (ANSI/IEEE Standard 176-1987 1988); p. 227-228.

Russell IJ, Kossl M. Micromechanical responses to tones in the auditory fovea of the greater mustached bat's cochlea. J. Neurophysiol 1999;82:676–686. [PubMed: 10444665]

Sherrit S, Widerick HD, Mukherjee BK, Sayer M. An accurate equivalent circuit for the unloaded piezoelectric vibrator in the thickness mode. J. Phys. D 1997;30:2354–2363.

Spector AA, Brownell WE, Popel AS. Estimation of elastic moduli and bending stiffness of the anisotropic outer hair cell wall. J. Acoust. Soc. Am 1998;103:1007–1011. [PubMed: 9479754]

Spector AA, Brownell WE, Popel AS. Nonlinear active force generation by cochlear outer hair cell. J. Acoust. Soc. Am 1999;105:2414–2420. [PubMed: 10212422]

Spector AA, Brownell WE, Popel AS. Effect of outer hair cell membrane piezoelectric properties on the receptor potential under high frequency conditions. J. Acoust. Soc. Am 2003;113:453–461. [PubMed: 12558282]

Spector, AA.; Popel, AS.; Brownell, WE. Piezoelectric properties enhance outer hair cell high-frequency response. In: Gummer, AW., editor. Biophysics of the Cochlea From Molecule to Model. World Scientific; Singapore: 2002. p. 152-160.

Tolomeo JA, Steele CR. Orthotropic piezoelectric properties of the cochlear outer hair cell wall. J. Acoust. Soc. Am 1995;97:3006–3011. [PubMed: 7601982]

White NR, Prasad M, Barfield RJ, Nyby JG. 40- and 70-kHz vocalizations of mice (Mus musculus) during copulation. Physiol. Behav 1998;63:467–473. [PubMed: 9523885]

Zhao HB, Santos-Sacchi J. Auditory collusion and a coupled couple of outer hair cells. Nature (London) 1999;399:359–362. [PubMed: 10360573]

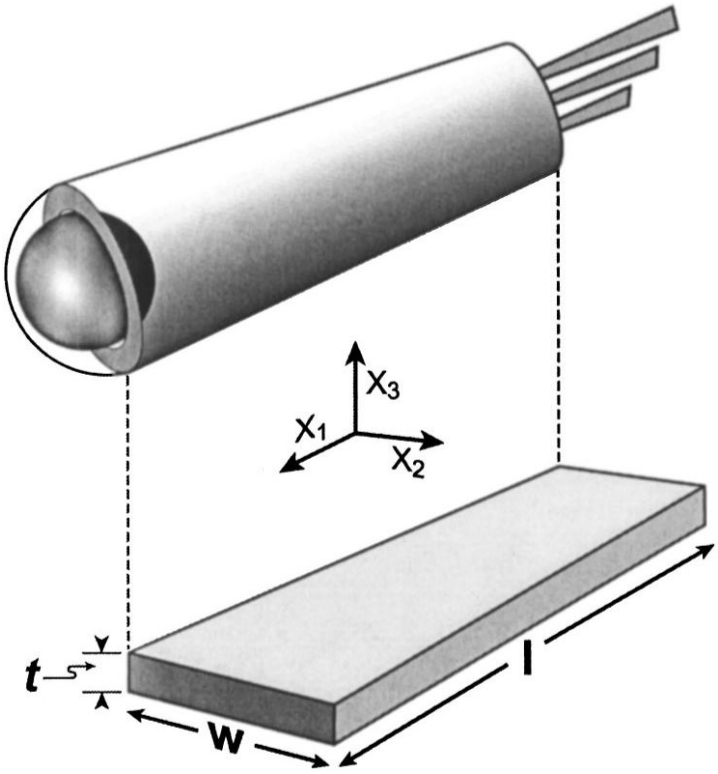

FIG. 1.
Schematic of cylindrical OHC lateral wall (above) and its LTE representation (below).

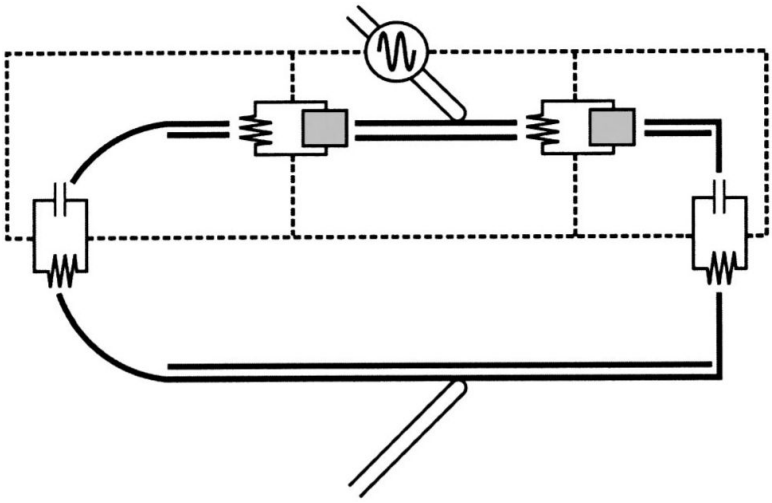

FIG. 2.

Equivalent circuit diagram for microchamber recording conditions. Gray box impedance in the lateral wall represents either a piezoelectric element [from Eq. (3)] or pure capacitance for the conventional RC analysis.

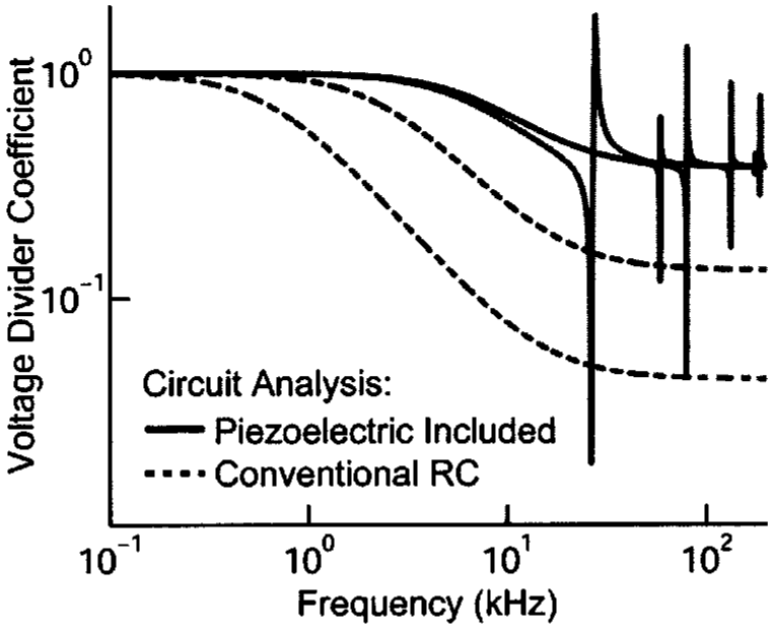

FIG. 3.

Equivalent circuit analysis for 20 and 80 μm OHCs with 1% of the cell in the microchamber. The solid and dashed gray lines with the lower cutoff and resonance frequency represent the 80 μm cell.

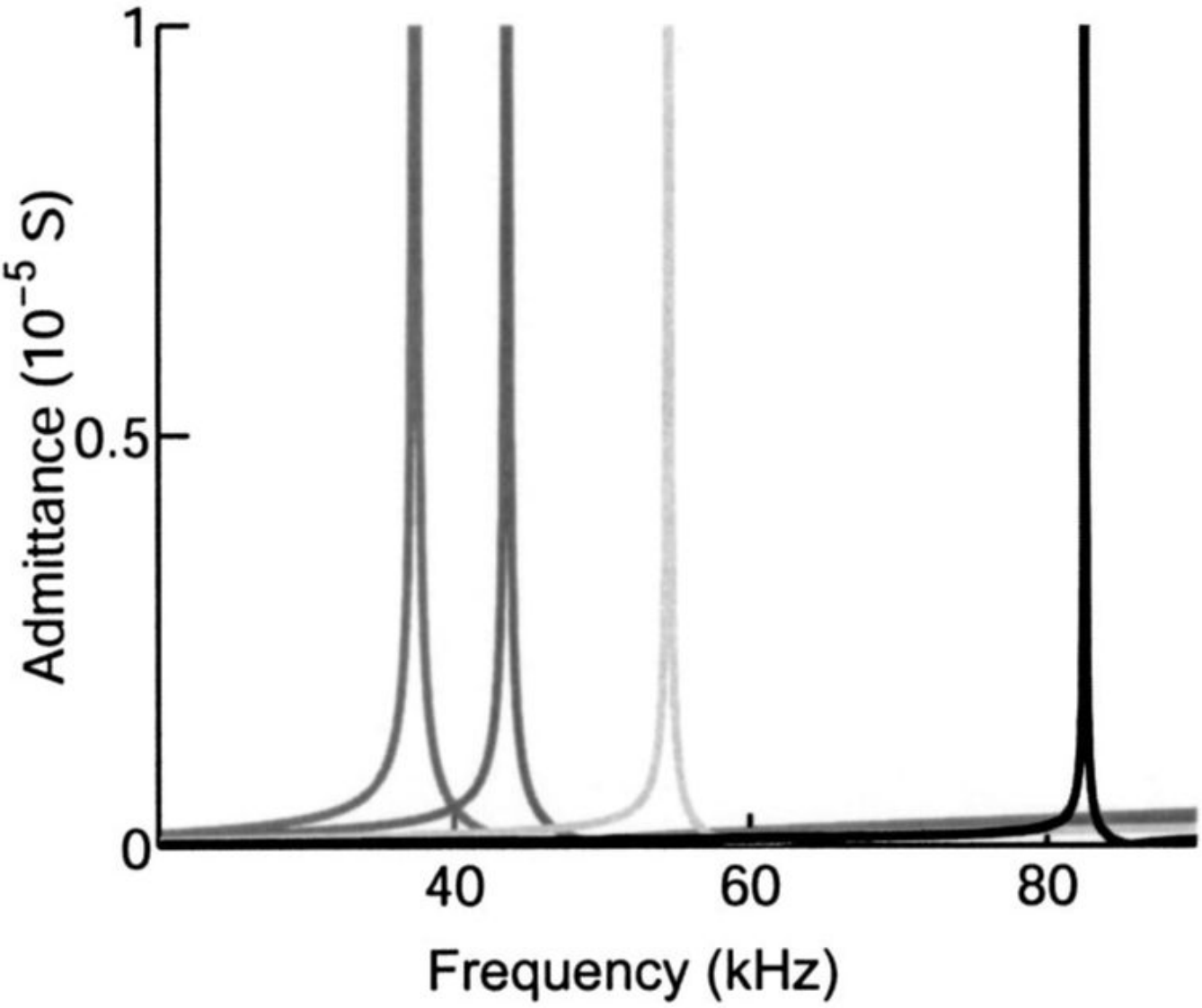

FIG. 4.

Admittance resonance peaks for LTE model of different lengths. The frequency of the resonance peaks are higher for shorter cells. The cell lengths are 80, 60, 40, and 20 μm proceeding from left to right.

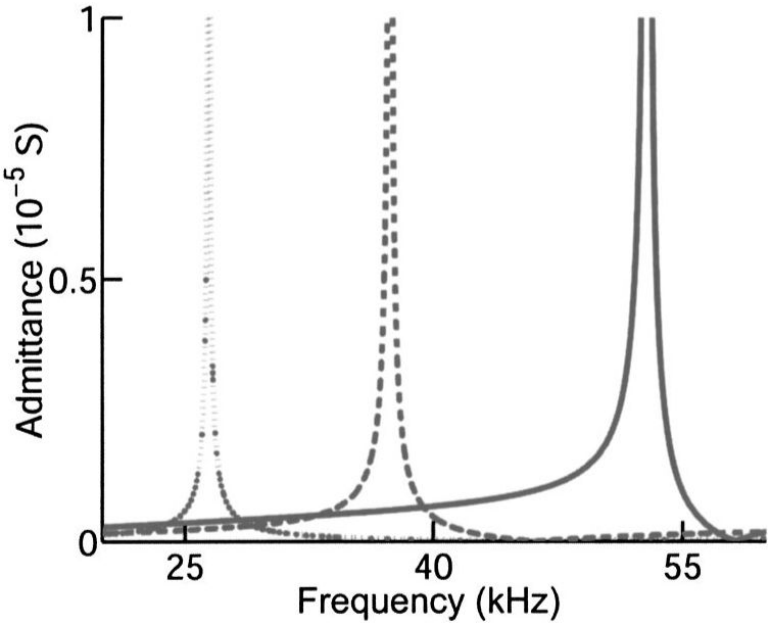

FIG. 5.

Effect of lateral wall thickness on admittance resonance spectrum for an LTE model of an 80-μm-long cell. All other parameters as in Fig. 4. Resonance frequency increases with decreasing thickness. The wall thickness is 200, 100, and 50 nm proceeding from left to right.

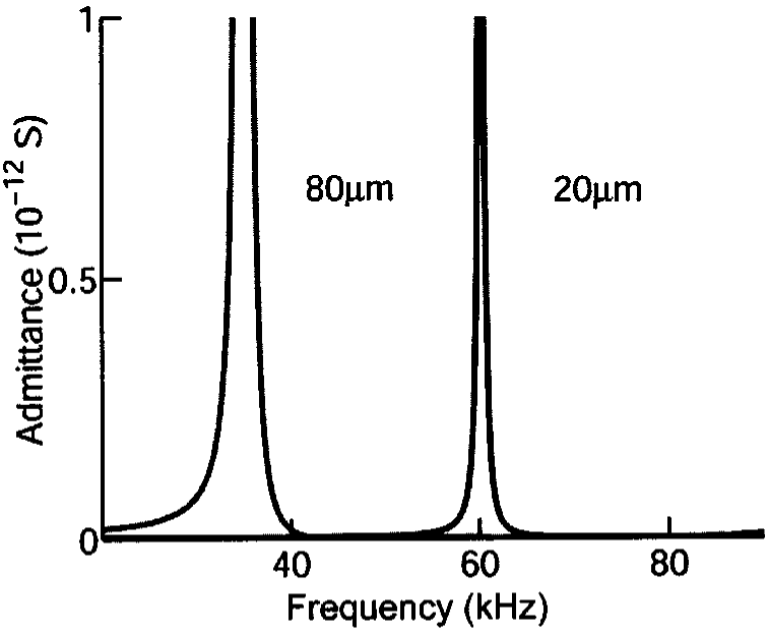

FIG. 6.

Radial poled cylinder (RPC) model. All parameters are the same as those used in the LTE model. The elastic compliance in the circumferential direction was chosen to be the same as that for the axial direction. Resonance frequency is similar to the LTE at 80 μm length, but at 20 μm length the resonance is not as high a frequency as that of the LTE model.

TABLE I

Coefficient values. LW—lateral wall; PE—piezoelectric

Coefficient	Symbol	Value	Unit
Length	l	20,40,60,80	μm
Radius	r	4.5	μm
Width (circumference)	w	28.5	μm
Thickness (LW & PE plate)	t	100[a]	nm
Density	ρ	1[a]	g/ml
PE plate permittivity	$\varepsilon_0 \varepsilon_{33}^{\mathrm{T}}$	5.0×10^{-11}	C^2/Nm^2
PE plate elastic compliance	s_{11}^{E}	3.1×10^{-5}	m^2/N
PE constant	d_{31}^2	6.8×10^{-16}	C^2/N^2
LW resistance	R_{pm}	100	Ωm^2
LW capacitance	C_{pm}	1.7×10^{-2}	F/m^2
Basal membrane resistance	R_{ba}	1	Ωm^2
Basal membrane capacitance	C_{ba}	1.7×10^{-2}	F/m^2
Apical area (cuticular plate)	A_{cp}	8.2×10^{-11}	m^2
Apical membrane resistance	R_{ap}	5.0×10^{-4}	Ωm^2
Apical membrane capacitance	C_{ap}	1.7×10^{-2}	F/m^2

[a]Estimated—this paper.